

Article

Facile Solution Spin-Coating SnO₂ Thin Film Covering Cracks of TiO₂ Hole Blocking Layer for Perovskite Solar Cells

Haiyan Ren, Xiaoping Zou *, Jin Cheng, Tao Ling, Xiao Bai and Dan Chen

Research Center for Sensor Technology, Beijing Key Laboratory for Sensor, Ministry of Education Key Laboratory for Modern Measurement and Control Technology, School of Applied Sciences, Jianxiangqiao Campus, Beijing Information Science & Technology University, Beijing 100101, China; yanh3100@gmail.com (H.R.); chengjin@bistu.edu.cn (J.C.); taoling8102@gmail.com (T.L.); aaiyan521@gmail.com (X.B.); danchen630@gmail.com (D.C.)

* Correspondence: hsh@mail.bistu.edu.cn; Tel.: +86-10-6488-4673 (ext. 816)

Received: 4 August 2018; Accepted: 3 September 2018; Published: 6 September 2018



Abstract: The hole blocking layer plays an important role in suppressing recombination of holes and electrons between the perovskite layer and fluorine-doped tin oxide (FTO). Morphological defects, such as cracks, at the compact TiO₂ hole blocking layer due to rough FTO surface seriously affect performance of perovskite solar cells (PSCs). Herein, we employ a simple spin-coating SnO₂ thin film solution to cover cracks of TiO₂ hole blocking layer for PSCs. The experiment results indicate that the TiO₂/SnO₂ complementary composite hole blocking layer could eliminate the serious electrical current leakage existing inside the device, extremely reducing interface defects and hysteresis. Furthermore, a high efficiency of 13.52% was achieved for the device, which is the highest efficiency ever recorded in PSCs with spongy carbon film deposited on a separated FTO-substrate as composite counter electrode under one sun illumination.

Keywords: perovskite solar cell; hole blocking layer; solution spin-coating; TiO₂/SnO₂ layer

1. Introduction

Currently, perovskite solar cells (PSCs) have been recognized as the most promising alternatives to conventional silicon solar cells due to high conversion efficiency, low manufacturing cost, and simple process [1–7]. As for typical planar heterojunction PSCs composed of working electrode (cathode)/hole blocking layer/perovskite layer/electron blocking layer/counter electrode (anode), the hole blocking layer plays an important role in extracting electrons from the perovskite layer and, as well as, suppressing recombination of holes and electrons between the perovskite layer and FTO [8–11]. A uniform, pinhole-free and well electrically conductive hole blocking layer is highly demanded for well performed planar heterojunction PSCs [8,12]. Liao et al. found that the pinholes on the surface of the single SnO₂ hole blocking layer coating on the rough FTO substrate were still hard to eliminate. Therefore, radio-frequency magnetron sputtering TiO₂ fully covered the surface of the FTO electrode, thus passivating the FTO surface defects and reducing the recombination, finally utilizing TiO₂/SnO₂ bilayer as hole blocking layer to improve device performance [8,13]. Furthermore, TiO₂ compact layer has commonly been used as the hole blocking layer in the planar heterojunction PSCs. Since the spin-coating process formed a highly irregular thick TiO₂ layer on top of the rough FTO layer, the pinholes appeared on the surface of the TiO₂ hole blocking layer, so that the perovskite light-absorber layer directly contacted the FTO layer, resulting in recombination of holes and electrons between the perovskite light-absorber layer and FTO layer. Though uniform and pinhole-free compact TiO₂ layers were prepared using atomic layer deposition to improve device performance, the atomic

layer deposition method had the disadvantage of including a low crystallinity of thin film due to the low deposition temperature [14]. However, Choi et al. mitigated the influence of the morphological defects (such as an irregular film thickness and poor physical contact between the TiO₂ and the FTO layers) at the TiO₂ interface due to a rough FTO by implementing a TiO₂ hole blocking layer based on the anodization method [15]. Though the research by Choi et al. mitigated the influence of the morphological defects, the preparation technology was very complicated. Up to now, several research groups have developed carbon counter electrodes to reduce the costs of perovskite devices [16–18]. In our research group, previously, the PSC based on sponge carbon/FTO composite counter electrode obtained the power conversion efficiency of 10.7% [19].

In this work, we employ TiO₂/SnO₂ complementary composite layer prepared by facile solution spin-coating SnO₂ on compact TiO₂-coated rough FTO as the hole blocking layer for planar heterojunction PSCs to solve morphological defects, such as cracks, at the compact TiO₂ hole blocking layer due to rough FTO surface. However, due to TiO₂ hole blocking layer has relative lower electron mobility, leading to unbalanced carrier transport in the device, thus regular planar structure PSC usually has a strong hysteresis behavior [20]. Meanwhile, SnO₂ is currently recognized as the promising hole blocking layer substitution for the conventional TiO₂ due to high electron mobility, low conduction band minimum, and low-temperature preparation [20–25]. Grätzel et al. and co-workers reported planar PSCs with efficiencies close to 21% using a simple, solution-processed technological approach for depositing SnO₂ layers [26]. Thereby, we obtained the modified hole blocking layer thin film without cracks through solution spin-coating SnO₂ on compact TiO₂-coated rough FTO at 3000 rpm. Correspondingly, this TiO₂/SnO₂ thin film and component optimization of perovskite precursor solution contributed to the formation of high-quality perovskite thin films (such as high crystallinity, large grain size, low defect density, and good flatness). Notably, the largest size of individual perovskite grain reached 2.67 μm. Therefore, PSC based on the TiO₂/SnO₂ complementary composite hole blocking layer achieved high power conversion efficiencies (PCE) of 13.52% in size of 0.2 cm² under absolute ambient condition, which is the highest efficiency ever recorded in PSCs with such spongy carbon/FTO composite counter electrode. These improvements indicate that the TiO₂/SnO₂ complementary composite hole blocking layer could eliminate the serious electrical current leakage existing inside the device and reduce interface defects.

2. Materials and Methods

2.1. Materials

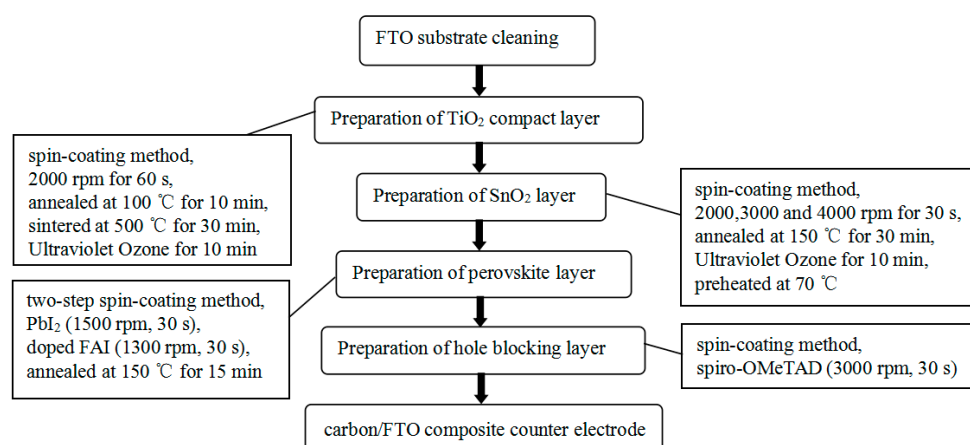
Fluorine-doped SnO₂ (FTO) substrates were obtained from Yingkou Opv Tech New Energy Co., Ltd. (Yingkou, China, 7–8 Ω/square, 2.2 mm in thickness, 1.5 × 1.5 cm² in specification). *N,N*-dimethylformamide (DMF) and dimethyl sulfoxide (DMSO) were purchased from Sa'en Chemical Technology (Shanghai, China) Co., Ltd. Acidic titanium dioxide solution (bl-TiO₂) was purchased from Shanghai MaterWin New Materials Co., Ltd. (Shanghai, China, product code of MTW-CL-H-002, commodity name of HH-TiO_x, colorless and transparent in appearance, 99.98% in purity). The SnO₂ colloid precursor (Cas No. 18282-10-5) was obtained from Alfa Aesar (Shanghai, China, tin (IV) oxide, 15% in H₂O colloidal dispersion). Before use, the particles were diluted by deionized water to 3%. Lead(II) Iodide (PbI₂, Cas No. 10101-63-0, yellow crystalline powder in appearance, purity >99.99%), Methylammonium iodide (CH₃NH₃I, MAI, Cas No. 14965-49-2, white powder in appearance, purity ≥99.5%), Formamidinium Iodide (HC(NH₂)₂I, FAI, Cas No. 879643-71-7, white powder in appearance, purity ≥99.5%), Methylammonium Bromide (CH₃NH₃Br, MABr, Cas No. 6876-37-5, white powder in appearance, purity ≥99.5%), Methylammonium Chloride (CH₃NH₃Cl, MACl, Cas No. 593-51-1, white powder in appearance, purity ≥99.5%), and commercial 2,2',7,7'-tetrakis-(*N,N*-dip-methoxyphenylamine)-9,9'-spirobifluorene solution (Spiro-OMeTAD, Cas No. 207739-72-8, yellow powder in appearance, purity ≥99.5%) were purchased from Xi'an Polymer Light Technology Corp. (Xi'an, China).

2.2. Device Fabrication

The surface treatment of the FTO for complete coverage before deposition of any film which affect severely the film deposition and properties. Malviya et al. demonstrated that rigorous cleaning process yielded clean FTO surface, and rigorous cleaning of the substrates prior to the hematite deposition was crucial for achieving highly reproducible results [27]. In order to ensure the quality of the subsequent film deposition, we thoroughly cleaned the FTO glass substrate before proceeding to the next step. FTO substrate was firstly wiped using a mixed solution of detergent and deionized water. The resultant FTO substrates were ultrasonically cleaned with glass water (deionized water: acetone: 2-propanol = 1:1:1) and ethanol for 20 min, separately. The FTO glasses were dried with dryer for 30 min and then cleaned with ultraviolet ozone for 10 min. Compact TiO₂ layer was deposited on the cleaned FTO substrate by spin-coating an acidic titanium dioxide solution at 2000 rpm for 60 s. The substrate was annealed on a hotplate at 100 °C for 10 min, and then sintered in muffle furnace at 500 °C for 30 min. For TiO₂/SnO₂ complementary composite hole blocking layer based devices, due to the hydrophobicity of the TiO₂ thin film layer and the complete aqueous solution of the SnO₂ precursor solution, the FTO/TiO₂ substrates were firstly cleaned by ultraviolet ozone for 10 min in order to form a hydrophilic group on the surface of the film. Then the SnO₂ functional layer was prepared by spin-coating 3 wt % SnO₂ precursor solution on the compact TiO₂-coated FTO substrate for 30 s at 2000, 3000, and 4000 rpm, respectively [23]. Subsequently, the FTO/TiO₂/SnO₂ based substrates were dried on a hotplate at 150 °C for 30 min, and then cleaned by ultraviolet ozone for 10 min again to improve its hydrophilicity.

The perovskite thin film was deposited by a two-step spin-coating method [19]. Firstly, the prepared FTO/TiO₂/SnO₂ substrates were preheated on a hotplate at 70 °C. The precursor solution of PbI₂ was prepared by dissolving 0.5993 g PbI₂ powder in 1 mL mixture of DMF/DMSO (0.95:0.05 of volume ratio), and then spin-coated on the preheated FTO/TiO₂/SnO₂ substrates at 1500 rpm for 30 s. After that, the doped FAI precursor solution was prepared by mixing 60 mg FAI and 6 mg MABr and 6 mg MACl in 1 mL isopropanol, and then spin-coated on the PbI₂ layer at 1300 rpm for 30 s. In order to obtain a high-quality perovskite light-absorber layer, the spin-coated substrates were annealed on a hotplate at 150 °C for 15 min under ambient condition. The electron blocking layer was deposited on top of the perovskite layer by 3000 rpm for 30 s using Spiro-OMeTAD solution.

Finally, some cleaned FTO glasses were used as substrates to collect soot of a burning candle as spongy carbon counter electrodes. The spongy carbon/FTO composite counter electrode was then pressed on the Spiro-OMeTAD layers of uncompleted devices. The whole process is carried out in air condition with a relative humidity of 10%–20% at room temperature. The entire preparation process was described in Scheme 1.



Scheme 1. The entire process of the device fabrication.

2.3. Characterization

X-ray diffraction (XRD) data from samples of perovskite films deposited on FTO/TiO₂/SnO₂ substrates were collected using an X-ray diffractometer (D8 Focus, Bruker, Dresden, Germany). The morphology of the perovskite films were measured using a scanning electron microscope (SEM) (SIGMA, Zeiss, Jena, Germany). The photo-current density–voltage (J – V) characteristics were measured under simulated standard air-mass AM 1.5 sunlight with using a solar simulator (Sol 3A, Oriol, Newport, RI, USA). All the measurements of the PSCs were performed under ambient atmosphere at room temperature without encapsulation.

3. Results and Discussion

Figure 1 shows the top-view SEM images of the bare FTO glass substrate (Figure 1a) and 3D roughness reconstruction of bare FTO glass (Figure 1f). As we can see, the surface of the bare FTO is very rough which corresponds to Sa (arithmetic-mean-height) of 74 nm. Many cracks (marked with a red square in Figure 1b) are observed on the surface of TiO₂ thin film. Figure 1c is the enlarged SEM surface image of the red square (in Figure 1b), however, the bottom FTO can be seen through the cracks, which will cause a large number of photocarriers to be recombination and seriously affect the performance of the PSC device. As shown in the cross-sectional SEM image (Figure 1d), the poor uniformity of TiO₂ thin film and the obvious fracture (marked with a red circle in Figure 1d) which was due to surface roughness of FTO, reveals that the bare FTO surface was exposed and could form direct contact with the perovskite layer, resulting in serious recombination of holes and electrons between the perovskite layer and FTO, in agreement with the results obtained with top-view SEM images (Figure 1b,c). The cross-sectional SEM image of bare FTO layer is shown in Figure 1e, we can find that the surface of bare FTO layer was very rough due to the presence of sharp peaks. Even some peaks and valleys reached a height of ~200 nm. However, as can be seen from Figure 1d, the spin-coating process formed a highly irregular thick TiO₂ layer due to overfilling the valleys on the rough FTO surface with TiO₂. The average thickness of single-layer TiO₂ compact layer was ~100 nm, which indicated some FTO peaks higher than 100 nm could not be covered, leading to the appearance of cracks in single-layer TiO₂ thin films. This is consistent with the observation from SEM images (Figure 1b,c) of the hole blocking layer thin films prepared with single-layer TiO₂ compact layer deposited on rough FTO substrates. The PSC devices based on single-layer TiO₂ hole blocking layer and double-layer TiO₂ hole blocking layer are named as device R1 and device R2, respectively. Table 1 shows the summary of J – V characteristics of device R1 and device R2 from reverse scan. As we can see, device R1 achieved low power conversion efficiency of 4.63% due to the presence of cracks. Compared with the device R1, the performance of the device R2 was improved. Huang et al. reported a facile dip-coating route to sequentially prepare a dense sol-gel-derived titanium dioxide (TiO₂) hole blocking layer and a smooth organolead halide perovskite film for pseudo-planar heterojunction perovskite solar cells [28]. Masood et al. used a scalable and low-cost dip coating method to prepare uniform and ultra-thin (5–50 nm) compact TiO₂ films on FTO glass substrates [29]. Though the dip-coating process does not require any complicated equipment and greatly minimizes the waste of source materials, enabling fast and easy production of uniform thin films, the method is not the same as our spin coating process.

Table 1. Summary of J – V characteristics of device R1 and device R2 from reverse scan.

Devices	N^a	J_{sc}^b (mA/cm ²)	V_{oc}^c (V)	FF ^d	PCE ^e (%)
R1	1	13.13	0.86	41.09	4.63
R2	2	18.26	0.97	54.70	9.66

Notes: ^a Number of TiO₂ spin-coating layers; ^b Short-circuit photocurrent density; ^c Open-circuit voltage; ^d Fill factor; ^e Power conversion efficiency.

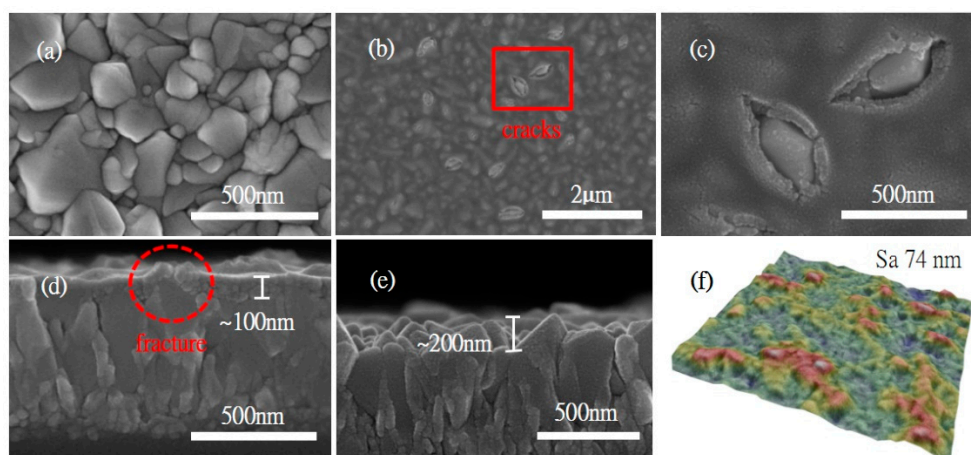


Figure 1. SEM images: (a) Top-view SEM image of bare FTO glass; (b,c) Top-view SEM image of TiO₂ film; (d) Cross-sectional SEM image of TiO₂ film; (e) Cross-sectional SEM image of bare FTO glass; (f) Top-view SEM image of 3D roughness reconstruction of bare FTO glass.

Figure 2 presents the top-view SEM images of SnO₂ thin films deposited on compact TiO₂-coated rough FTO for 30 s at 2000 rpm (Figure 2a,b), 3000 rpm (Figure 2c,d), and 4000 rpm (Figure 2e,f), respectively. As shown in Figure 2a,b, the cracks on the surface of the TiO₂/SnO₂ thin film were obviously filled with SnO₂ crystal grains. Due to the rotational speed being too low, a thick SnO₂ thin film formed. Thus, many cracks appeared on the surface of the SnO₂ thin film. Jiang et al. demonstrated a dense, pinhole-free film formed by spin coating SnO₂ nanoparticles solution onto glass/Indium-Tin Oxide (ITO) substrate at 3000 rpm [23]. However, in our experiment, as shown in Figure 2c,d, modified TiO₂/SnO₂ thin film without visible cracks through solution spin-coating SnO₂ on compact TiO₂-coated rough FTO at 3000 rpm formed, and is flat, uniform, and dense, which indicates the TiO₂/SnO₂ complementary composite hole blocking layer is able to fully cover the rough surface of the FTO electrode. Choi et al. demonstrated the TiO₂ film was so too thin that pinholes were observed in the TiO₂ layer, and electrons in the FTO layer easily recombined with holes due to the lack of hole blocking [15]. However, in our experiment, as the rotating speed increased to 4000 rpm, the bare FTO was exposed from a few large cracks in Figure 2e,f, which indicated that the thickness of the functional layer of SnO₂ was thinner due to the excessive spin-coating speed, and coverage of FTO/TiO₂ based substrate is incomplete. This result suggests that the direct contact between bare FTO and the perovskite light-absorber layer can cause the recombination of holes and electrons, leading to the degradation of device performance. It is consistent with the results obtained with summary of photovoltaic parameters with the *J-V* characteristics from reverse scan of the PSC devices based on TiO₂/SnO₂ complementary composite hole blocking layer.

However, the reasons for formation of cracks are different under high speed (4000 rpm) and low speed (2000 rpm), presented in detail in Figure 3. Figure 3 presents schematics for formation process of SnO₂ thin films at different rotational speed. Compared with situations of other rotational speed, the SnO₂ thin film from 2000 rpm was thicker, and the total amount of solution in the film was more. The solvent volatilization rate is lower during the spin coating process of 30 s, so that the solution film of SnO₂ was formed. During the annealing process of the solution film at 150 °C for 30 min, the solvent evaporated and the solution film contracted in the thickness direction, resulting in the exposure of the sharp peak of substrate, thus forming the cracks, as shown as Figure 3, corresponding to the SEM images (Figure 2a,b).

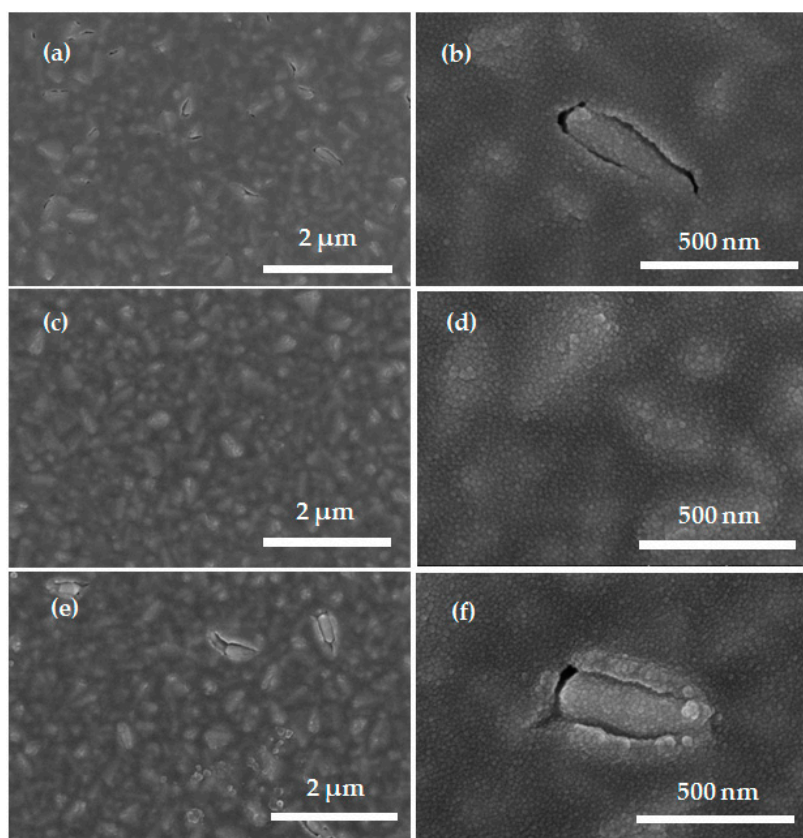


Figure 2. Top-view SEM images of SnO₂ thin films deposited on compact TiO₂-coated rough FTO at different spin-coating speeds for 30 s: (a,b) 2000 rpm; (c,d) 3000 rpm; (e,f) 4000 rpm.

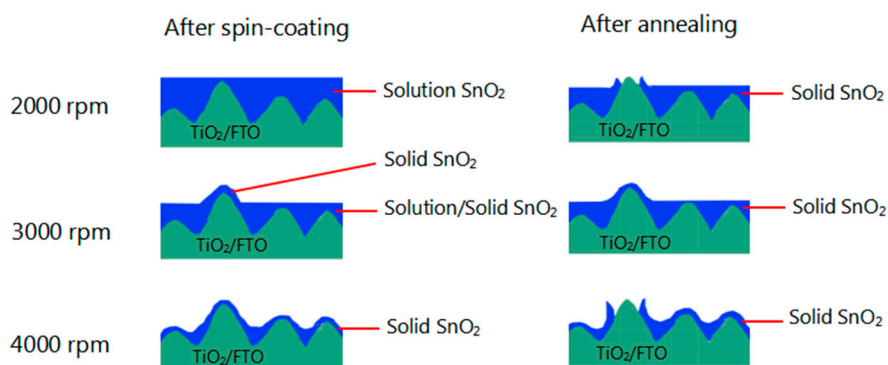


Figure 3. Schematics for formation of SnO₂ thin films at different rotational speed.

For the SnO₂ film from 3000 rpm, the solvent volatilized rate was more than the situation of SnO₂ film from 2000 rpm during the spin coating of 30 s, and the film itself was relatively thinner, thus forming a semi-solid/semi-liquid film after finishing the spin coating. In particular, the SnO₂ film at the location of the sharp peak of substrate almost became solid, thus preserving the shape at the location of the sharp peak, as shown as Figure 3, corresponding to the SEM images (Figure 2c,d).

In the process of spin-coating at 4000 rpm, the solvent volatilization was very fast, and the whole SnO₂ film was very thin and the total amount of solvent was very little, so the solid SnO₂ film had been formed after 30 s spin coating. It is worth noting that at the position of the sharp peak of substrate, the SnO₂ film was so thin that the ability to withstand strain of the film was very weak, resulting in a crack after annealing at 150 °C, as shown as Figure 3, corresponding to the SEM images (Figure 2e,f).

In addition, the film from spin coating at high speed was thinner than the one at low speed, and the film from spin coating at high speed was rougher than the one at low speed. Light trapping is a technique to improve optical absorption in the active layer of a solar cell. The rough surface can act as a light trapping structure to enhance the absorption perovskite solar cell [30–33]. However, the feature size here (<74 nm) is far less than the effective trapping sizes mentioned by previous research groups (~300 nm [30], ~6 μm [31] and ~800 nm [32]), so that the $\text{TiO}_2/\text{SnO}_2$ thin film with lower roughness is not the main reason for the efficiency drop.

Figure 4 presents the cross-sectional SEM images of the $\text{TiO}_2/\text{SnO}_2$ complementary composite hole blocking layer with SnO_2 spin-coated on compact TiO_2 -coated FTO at 3000 rpm, which indicated the formation of modified $\text{TiO}_2/\text{SnO}_2$ film without visible breakages. As shown in Figure 4a, the entire film of $\text{TiO}_2/\text{SnO}_2$ complementary composite hole blocking layer was uniform in thickness and completely covered. Compared with single-layer TiO_2 hole blocking layer thin film, the SnO_2 thin film spin-coated on compact TiO_2 -coated rough FTO exhibited a flatter surface. Notably, as shown in Figure 4b, the $\text{TiO}_2/\text{SnO}_2$ complementary composite hole blocking layer also has good coverage at the protrusions of the underlying substrate and no breakage or large bulging in the protrusions could be observed. This is consistent with the observation from top-view SEM images of SnO_2 films deposited on compact TiO_2 -coated rough FTO at 3000 rpm (Figure 2c,d).

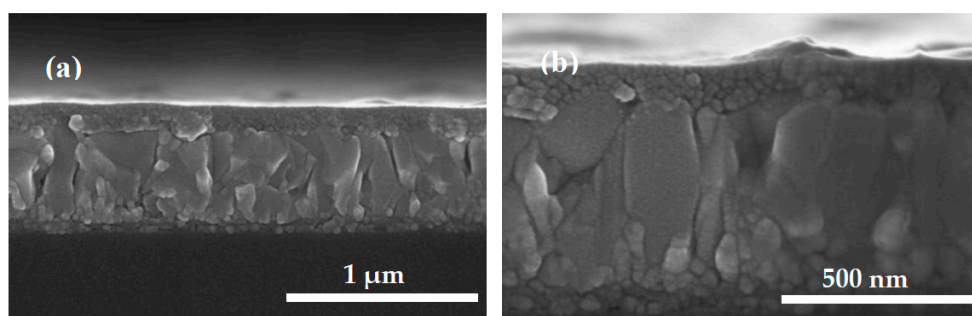


Figure 4. Cross-sectional SEM images of the $\text{TiO}_2/\text{SnO}_2$ complementary composite hole blocking layer with SnO_2 spin-coated on compact TiO_2 -coated rough FTO at 3000 rpm: (a) Smaller magnification; (b) Larger magnification.

Figure 5 shows schematic illustration for the solution spin-coating process of $\text{TiO}_2/\text{SnO}_2$ complementary composite hole blocking layer. As we can see, the surface of the bare FTO was very rough due to the presence of sharp peaks (Figure 5a), corresponding to the SEM image (Figure 1e). As shown in Figure 5b, the spin-coating process formed a highly irregular thick TiO_2 layer due to overfilling the valleys on the rough FTO surface with TiO_2 , resulting in many cracks appearing on the surface of TiO_2 , and the bare FTO surface was exposed, corresponding to the SEM images (Figure 1b–d). However, as can be seen from Figure 5c, the cracks were absent from the surface of SnO_2 thin film deposited on compact TiO_2 -coated rough FTO at 3000 rpm and the SnO_2 thin film fully covered the surface of the FTO electrode, corresponding to the SEM images (Figure 2c,d). Meanwhile, the SnO_2 thin film is flat, uniform, and dense, corresponding to the SEM images (Figure 4). This result suggests that the modified $\text{TiO}_2/\text{SnO}_2$ complementary composite hole blocking layer is beneficial to suppressing recombination of holes and electrons between the perovskite layer and FTO and enhances the performance of devices.

XRD data of the SnO_2 thin film deposited on FTO/ TiO_2 substrate were collected in Figure 6. Each of the marked peak positions in the figure (Figure 6) corresponded to the (110), (101), (200), (211), (310), (301) crystal planes of the SnO_2 crystal, which was in consistent with the results of the previous report [23] about XRD pattern of the SnO_2 material, indicating SnO_2 thin film composite counter electrodes had been successfully deposited on the FTO/ TiO_2 substrate.

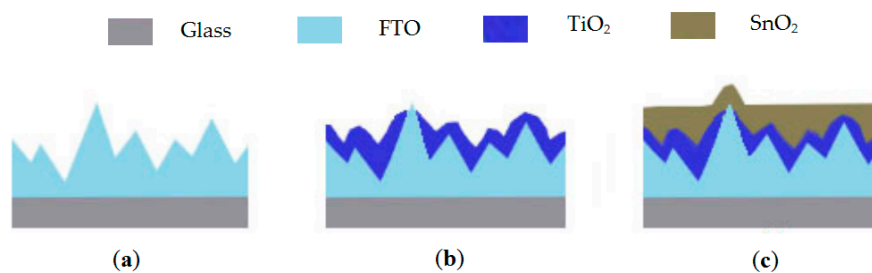


Figure 5. Schematic illustration for the solution spin-coating process of TiO₂/SnO₂ complementary composite hole blocking layer: (a) The bare FTO substrate; (b) TiO₂ thin film deposited on rough FTO substrate; (c) SnO₂ thin film deposited on compact TiO₂-coated rough FTO at 3000 rpm.

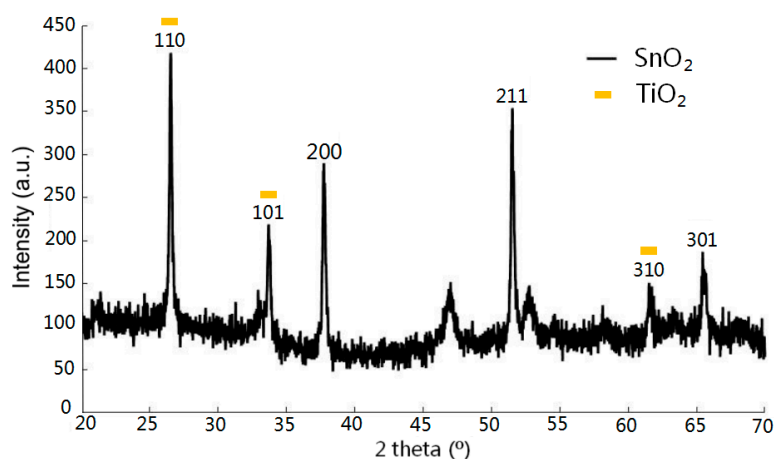


Figure 6. XRD pattern of SnO₂ thin film deposited on FTO/TiO₂ substrate.

Figure 7 presents top-view SEM images (Figure 7a,b) and cross-sectional SEM image (Figure 7c) of perovskite thin films deposited on TiO₂/SnO₂ of solution spin-coating SnO₂ on compact TiO₂-coated rough FTO at 3000 rpm, respectively. From Figure 7a,b, it can be seen that the entire perovskite film was high-quality and quite uniform free of cracks. However, high-quality perovskite film is essential for the performance of planar PSCs, as it can avoid the direct contact of hole blocking layer and electron blocking layer [20]. It is worth noting that the individual grain size of perovskite crystals was especially large, and the largest grain size reached a rare 2.67 μm . Furthermore, due to the passivation of the doping, the grain boundary was too smooth, which reduced defects of grain boundaries in the perovskite film to a great extent. From the cross-sectional SEM image (Figure 7c), it can be found that the entire perovskite film was composed of single layer of large grains and uniformly dense, which is coincident with the morphology of the film on the top-view SEM images (Figure 7a,b).

Figure 8 displays the XRD pattern of the perovskite thin film deposited on FTO/TiO₂/SnO₂ substrate in the case of spin-coating SnO₂ at 3000 rpm. Obviously, the XRD pattern presents strong and sharp (101) and (200) diffraction peaks at 14.02° and 28.32°, demonstrating the good crystallinity of perovskite film, which is consistent with the SEM results (Figure 7) of the large-grain-size perovskite film. The perovskite grains of good crystallinity effectively enhance the efficiency of injection of photo-carriers of the perovskite light-absorber layer into the hole blocking layer and electron blocking layer, thereby further improving the overall performance of the PSC device.

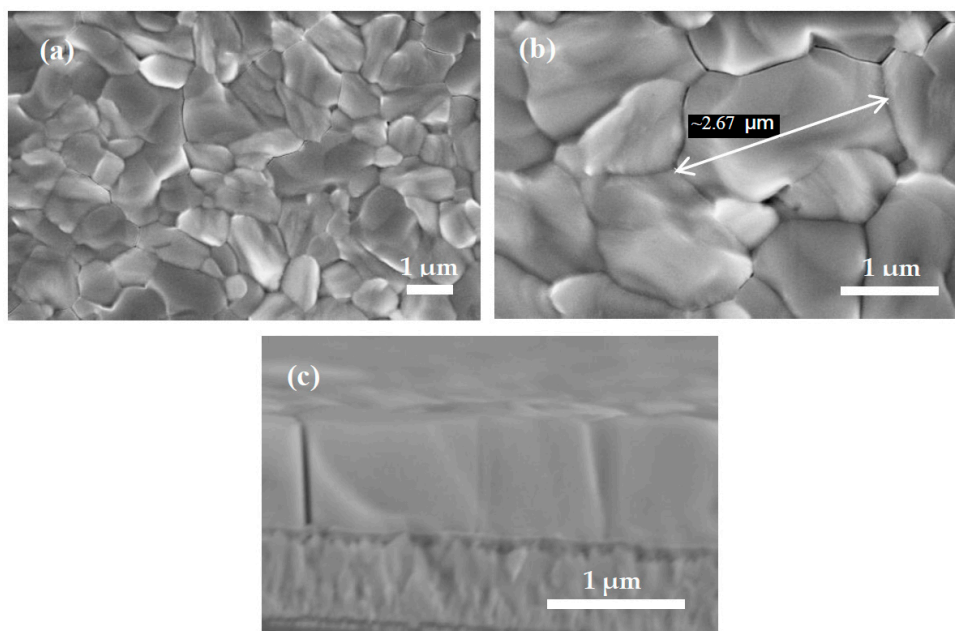


Figure 7. SEM images: (a,b) Top-view SEM images of FTO/TiO₂/SnO₂/perovskite; (c) Cross-sectional SEM image of FTO/TiO₂/SnO₂/perovskite.

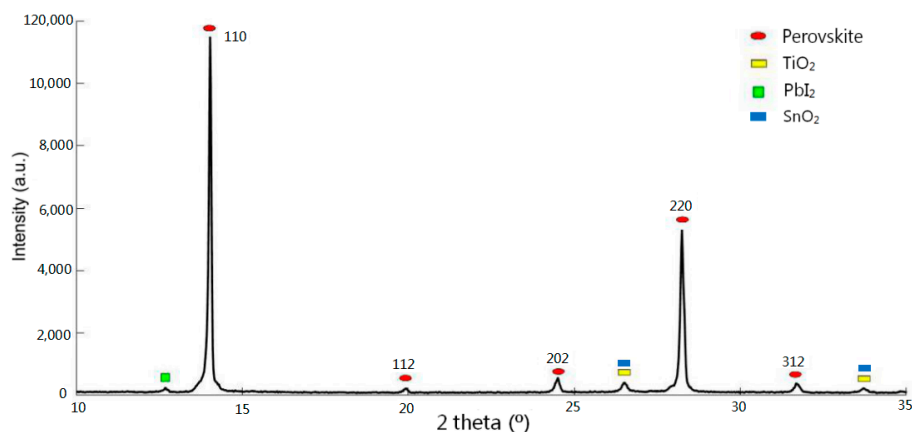


Figure 8. XRD pattern of the perovskite thin film deposited on FTO/TiO₂/SnO₂ substrate in the case of spin-coating SnO₂ at 3000 rpm.

Figure 9 shows energy bandgap diagram for TiO₂/SnO₂ based PSC, the shift of conduction band is not the main reason for the efficiency drop [34].

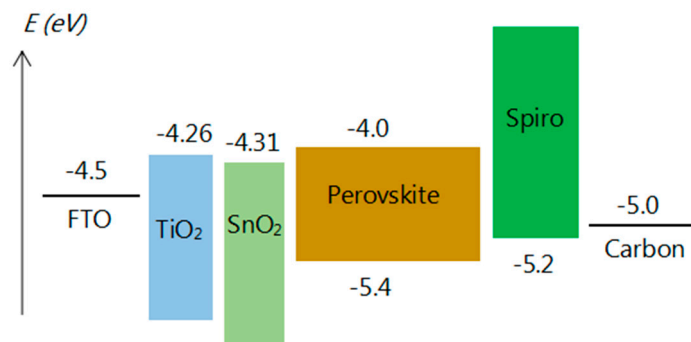


Figure 9. Energy bandgap diagram for TiO₂/SnO₂ based perovskite solar cells.

Figure 10 shows the J - V curves from reverse scan (RS) and forward scan (FS) for the PSC devices based on $\text{TiO}_2/\text{SnO}_2$ complementary composite hole blocking layer under different SnO_2 spin-coating speeds, measured under simulated sunlight with intensity of 100 mW cm^{-2} (AM 1.5 G). Obviously, when the SnO_2 spin-coating speed was 3000 rpm, the RS and FS curves of the device basically coincided and the hysteresis phenomenon basically disappeared, which matches the thin film morphology seen from the top-view SEM images (Figure 7a,b). When the SnO_2 spin-coating speeds were 2000 and 4000 rpm, a SnO_2 functional layer that was wither too thick or too thin could not match well with the TiO_2 compact layer to form modified $\text{TiO}_2/\text{SnO}_2$ complementary composite hole blocking layer. This led directly to a drop in the optoelectronic performance of the device. The presence of cracks also caused serious electrical current leakage existing inside the device, resulting the PSC devices under these two processes having different degrees of hysteresis.

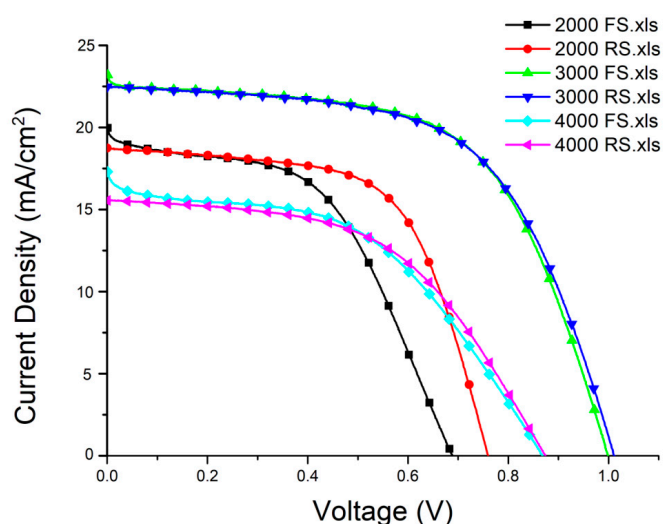


Figure 10. The J - V curves from reverse scan (RS) and forward scan (FS) for the PSC devices based on $\text{TiO}_2/\text{SnO}_2$ complementary composite hole blocking layer under different SnO_2 spin-coating speeds, measured under simulated sunlight with intensity of 100 mW cm^{-2} (AM 1.5 G).

Table 2 shows summary of J - V characteristics from RS of the PSC devices based on $\text{TiO}_2/\text{SnO}_2$ complementary composite hole blocking layer under different SnO_2 spin-coating speeds. The best cell based on $\text{TiO}_2/\text{SnO}_2$ complementary composite hole blocking layer under the SnO_2 spin-coating speed of 3000 rpm obtained a PEC of 13.52% corresponding to a J_{sc} of 22.48 mA cm^{-2} , a V_{oc} of 1.01 V and a FF of 59.51. Although this efficiency is not the highest in PSCs, it is the highest efficiency ever recorded in PSCs with such spongy carbon/FTO composite counter electrode, and furthermore, the preparation techniques of high-quality perovskite thin films and the cheap spongy carbon/FTO composite counter electrode under absolute ambient condition are beneficial for large-scale applications and commercialization. At the same time, since the problem of the defect at the interface between the hole blocking layer and the perovskite light-absorber layer was solved, the hysteresis phenomenon of the entire device was well solved.

Table 2. Summary of J - V characteristics from reverse scan of the PSC devices based on $\text{TiO}_2/\text{SnO}_2$ complementary composite hole blocking layer under different SnO_2 spin-coating speeds.

RSSC ^a (rpm)	J_{sc} ^b (mA/cm^2)	V_{oc} ^c (V)	FF ^d	PCE ^e (%)
2000	18.74	0.76	61.95	8.81
3000	22.48	1.01	59.51	13.52
4000	15.56	0.87	52.22	7.10

Notes: ^a Rotating speed of spin-coating SnO_2 ; ^b Short-circuit photocurrent density; ^c Open-circuit voltage; ^d Fill factor; ^e Power conversion efficiency.

4. Conclusions

In summary, we optimized a rotational speed of spin-coating SnO₂ at 3000 rpm to cover the cracks of compact TiO₂-coated on rough FTO. Using composite layered TiO₂/SnO₂ can reduce hysteresis behavior due to an effectively suppressed recombination of holes and electrons between the perovskite layer and FTO. Meanwhile, as a result, we achieved high-quality perovskite thin films and high efficiency of 13.52% for devices with spongy carbon/FTO composite counter electrode. This work highlights the preparation process of modified hole blocking layer in PSC and has a certain reference significance for perovskite based opto-electronic devices.

Author Contributions: Conceptualization, X.B.; Methodology, X.Z.; Validation, D.C.; Investigation, H.R.; Data Curation, J.C.; Writing-Original Draft Preparation, H.R.; Writing-Review & Editing, T.L.; Visualization, H.R.; Supervision, X.Z.

Funding: This research was funded by Project of Natural Science Foundation of China (No. 61875186), Project of Natural Science Foundation of Beijing (No. Z160002), Opened Fund of the State Key Laboratory on Integrated Optoelectronics (No. IOSKL2016KF19), and Beijing Key Laboratory for Sensors of BISTU (No. KF20181077203).

Conflicts of Interest: The authors declare no conflicts of interest.

References

1. Snaith, H.J. Perovskites: The emergence of a new Era for low-cost, high-efficiency solar cells. *J. Phys. Chem. Lett.* **2013**, *4*, 3623–3630. [[CrossRef](#)]
2. Park, N.G. Organometal perovskite light absorbers toward a 20% efficiency low-cost solid-state mesoscopic solar cell. *J. Phys. Chem. Lett.* **2013**, *4*, 2423–2429. [[CrossRef](#)]
3. Green, M.A.; Ho-Baillie, A.; Snaith, H.J. The emergence of perovskite solar cells. *Nat. Photonics* **2014**, *8*, 506–514. [[CrossRef](#)]
4. Grätzel, M. The light and shade of perovskite solar cells. *Nat. Mater.* **2014**, *13*, 838–842. [[CrossRef](#)] [[PubMed](#)]
5. Abdi-Jalebi, M.; Pazoki, M.; Philippe, B.; Dar, M.I.; Alsari, M.; Sadhanala, A.; Diyitini, G.; Imani, R.; Lilliu, S.; Kullgren, J.; et al. Dedoping of lead halide perovskites incorporating monovalent cations. *ACS Nano* **2018**, *12*, 7301–7311. [[CrossRef](#)] [[PubMed](#)]
6. Alsari, M.; Bikondoa, O.; Bishop, J.; Abdi-Jalebi, M.; Ozer, L.Y.; Hampton, M.; Thompson, P.; Horantner, M.T.; Mahesh, S.; Greenland, C.; et al. In situ simultaneous photovoltaic and structural evolution of perovskite solar cells during film formation. *Energy Environ. Sci.* **2018**, *11*, 383–393. [[CrossRef](#)]
7. Alsari, M.; Pearson, A.J.; Wang, J.T.W.; Wang, Z.P.; Montisci, A.; Greenham, N.C.; Snaith, H.J.; Lilliu, S.; Friend, H. Degradation kinetics of inverted perovskite solar cells. *Sci. Rep.* **2018**, *8*, 5977. [[CrossRef](#)] [[PubMed](#)]
8. Liu, Z.Y.; Sun, B.; Liu, X.Y.; Han, J.H.; Ye, H.B.; Tu, Y.X.; Chen, C.; Shi, T.L.; Lang, Z.R.; Liao, G.L. 15% efficient carbon based planar-heterojunction perovskite solar cells using TiO₂/SnO₂ bilayer as electron transport layer. *J. Mater. Chem. A* **2018**, *6*, 7409–7419. [[CrossRef](#)]
9. Ren, Z.Q.; Wang, N.; Zhu, M.H.; Li, X.; Qi, J.Y. A NH₄F interface passivation strategy to produce air-processed high-performance planar perovskite solar cells. *Electrochim. Acta* **2018**, *282*, 653–661. [[CrossRef](#)]
10. Li, X.; Yang, J.Y.; Jiang, Q.H.; Lai, H.; Li, S.P.; Xin, J.W.; Chu, W.J.; Hou, J.D. Low-temperature solution-processed znse electron transport layer for efficient planar perovskite solar cells with negligible hysteresis and improved photostability. *ACS Nano* **2018**, *12*, 5605–5614. [[CrossRef](#)] [[PubMed](#)]
11. Ma, J.J.; Yang, G.; Qin, M.C.; Zheng, X.L.; Lei, H.W.; Chen, C.; Chen, Z.L.; Guo, Y.X.; Han, H.W.; Zhao, X.Z.; et al. MgO nanoparticle modified anode for highly efficient SnO₂-based planar perovskite solar cells. *Adv. Sci.* **2017**, *4*, 1700031. [[CrossRef](#)] [[PubMed](#)]
12. Wu, Y.Z.; Yang, X.D.; Chen, H.; Zhang, K.; Qin, C.J.; Liu, J.; Peng, W.Q.; Islam, A.; Bi, E.B.; Ye, F.; et al. Highly compact TiO₂ layer for efficient hole-blocking in perovskite solar cells. *Appl. Phys. Express* **2014**, *7*, 052301. [[CrossRef](#)]
13. Liu, Y.; Peng, Q.; Zhou, Z.P.; Yang, G. Effects of substrate temperature on properties of transparent conductive Ta-doped TiO₂ films deposited by radio-frequency magnetron sputtering. *Chin. Phys. Lett.* **2018**, *35*, 048101. [[CrossRef](#)]

14. Duong, T.T.; Kim, Y.J.; Eom, J.H.; Choi, J.S.; Le, A.T.; Yoon, S.G. Enhancement of solar cell efficiency using perovskite dyes deposited via a two-step process. *RSC Adv.* **2015**, *5*, 33515–33523. [[CrossRef](#)]
15. Choi, J.; Song, S.; Horantner, M.T.; Snaith, H.J.; Park, T. Well-defined nanostructured, single-crystalline TiO₂ electron transport layer for efficient planar perovskite solar cells. *ACS Nano* **2016**, *10*, 6029–6036. [[CrossRef](#)] [[PubMed](#)]
16. Zhang, N.; Guo, Y.; Yin, X.; He, M.; Zou, X. Spongy carbon film deposited on a separated substrate as counter electrode for perovskite-based solar cell. *Mater. Lett.* **2016**, *182*, 248–252. [[CrossRef](#)]
17. Mei, A.; Li, X.; Liu, L.; Ku, Z.; Liu, T.; Rong, Y.G.; Xu, M.; Hu, M.; Chen, J.; Yang, Y.; et al. A hole-conductor-free, fully printable mesoscopic perovskite solar cell with high stability. *Science* **2014**, *345*, 295–298. [[CrossRef](#)] [[PubMed](#)]
18. Habisreutinger, S.N.; Leijtens, T.; Eperon, G.E.; Stranks, S.D.; Nicholas, R.J.; Snaith, H.J. Carbon nanotube/polymer composites as a highly stable hole collection layer in perovskite solar cells. *Nano Lett.* **2014**, *14*, 5561–5568. [[CrossRef](#)] [[PubMed](#)]
19. Ling, T.; Zou, X.P.; Cheng, J.; Bai, X.; Ren, H.Y.; Chen, D. Modified sequential deposition route through localized-liquid-liquid-diffusion for improved perovskite multi-crystalline thin films with micrometer-scaled grains for solar cells. *Nanomaterials* **2018**, *8*, 416. [[CrossRef](#)] [[PubMed](#)]
20. Wu, C.C.; Huang, Z.R.; He, Y.H.; Luo, W.; Ting, H.K.; Li, T.Y.; Sun, W.H.; Zhang, Q.H.; Chen, Z.J.; Xiao, L.X. TiO₂/SnO_xCl_y double layer for highly efficient planar perovskite solar cells. *Org. Electron.* **2017**, *50*, 485–490. [[CrossRef](#)]
21. Ke, W.J.; Fang, G.J.; Liu, Q.; Xiong, L.B.; Qin, P.L.; Tao, H.; Wang, J.; Lei, W.H.; Li, B.R.; Wan, J.W.; et al. Low-temperature solution-processed tin oxide as an alternative electron transporting layer for efficient perovskite solar cells. *J. Am. Chem. Soc.* **2015**, *137*, 6730–6733. [[CrossRef](#)] [[PubMed](#)]
22. Song, J.X.; Zheng, E.Q.; Bian, J.; Wang, X.F.; Tian, W.J.; Sanehira, Y.; Miyasaka, T. Low-temperature SnO₂-based electron selective contact for efficient and stable perovskite solar cells. *J. Mater. Chem. A* **2015**, *3*, 10837–10844. [[CrossRef](#)]
23. Jiang, Q.; Zhang, L.Q.; Wang, H.L.; Yang, X.L.; Meng, J.H.; Liu, H.; Yin, Z.G.; Wu, J.L.; Zang, X.W.; You, J.B. Enhanced electron extraction using SnO₂ for high-efficiency planar-structure HC(NH₂)₂PbI₃-based perovskite solar cells. *Nat. Energy* **2017**, *2*, 16177. [[CrossRef](#)]
24. Baena, J.P.C.; Steier, L.; Tress, W.; Saliba, M.; Neutzner, S.; Matsui, T.; Giordano, F.; Jacobsson, T.J.; Kandada, A.R.S.; Zakeeruddin, S.M.; et al. Highly efficient planar perovskite solar cells through band alignment engineering. *Energy Environ. Sci.* **2015**, *8*, 2928–2934. [[CrossRef](#)]
25. Chen, J.Y.; Chueh, C.C.; Zhu, Z.L.; Chen, W.C.; Jen, A.K.Y. Low-temperature electrodeposited crystalline SnO₂ as an efficient electron transporting layer for conventional perovskite solar cells. *Sol. Energy Mater. Sol. Cells* **2017**, *164*, 47–55. [[CrossRef](#)]
26. Anaraki, E.H.; Kermanpur, A.; Steier, L.; Domanski, K.; Matsui, T.; Tress, W.; Saliba, M.; Abate, A.; Grätzel, M.; Hagfeldt, A.; et al. Highly efficient and stable planar perovskite solar cells by solution-processed tin oxide. *Energy Environ. Sci.* **2016**, *9*, 3128–3134. [[CrossRef](#)]
27. Malviya, K.D.; Dotan, H.; Yoon, K.R.; Kim, I.D.; Rothschild, A. Rigorous substrate cleaning process for reproducible thin film hematite (alpha-Fe₂O₃) photoanodes. *J. Mater. Res.* **2016**, *31*, 1565–1573. [[CrossRef](#)]
28. Huang, L.K.; Li, C.; Sun, X.X.; Xu, R.; Du, Y.Y.; Ni, J.; Cai, H.K.; Li, J.; Hu, Z.Y.; Zhang, J.J. Efficient and hysteresis-less pseudo-planar heterojunction perovskite solar cells fabricated by a facile and solution-saving one-step dip-coating method. *Org. Electron.* **2017**, *40*, 13–23. [[CrossRef](#)]
29. Masood, M.T.; Weinberger, C.; Sarfraz, J.; Rosqvist, E.; Sanden, S.; Sandberg, O.J.; Vivo, P.; Hashmi, G.; Lund, P.D.; Osterbacka, R.; et al. Impact of film thickness of ultrathin dip-coated compact TiO₂ layers on the performance of mesoscopic perovskite solar cells. *ACS Appl. Mater. Interfaces* **2017**, *9*, 17906–17913. [[CrossRef](#)] [[PubMed](#)]
30. Du, Q.G.; Shen, G.S.; John, S. Light-trapping in perovskite solar cells. *AIP Adv.* **2016**, *6*, 065002. [[CrossRef](#)]
31. Iftiqar, S.M.; Yi, J.S. Numerical simulation and light trapping in perovskite solar cell. *J. Photonics Energy* **2016**, *6*, 025507. [[CrossRef](#)]
32. Peer, A.; Biswas, R.; Park, J.M.; Shinar, R.; Shinar, J. Light management in perovskite solar cells and organic LEDs with microlens arrays. *Opt. Express* **2017**, *25*, 10704–10709. [[CrossRef](#)] [[PubMed](#)]

33. Bhattacharya, J.; Peer, A.; Joshi, P.H.; Biswas, R.; Dalal, V.L. Blue photon management by inhouse grown ZnO:Al cathode for enhanced photostability in polymer solar cells. *Sol. Energy Mater. Sol. Cells* **2018**, *179*, 95–101. [[CrossRef](#)]
34. Lee, Y.H.; Paek, S.; Cho, K.T.; Oveisi, E.; Gao, P.; Lee, S.; Park, J.S.; Zhang, Y.; Humphry-Baker, R.; Asiri, A.M.; et al. Enhanced charge collection with passivation of the tin oxide layer in planar perovskite solar cells. *J. Mater. Chem. A* **2017**, *5*, 12729–12734. [[CrossRef](#)]



© 2018 by the authors. Licensee MDPI, Basel, Switzerland. This article is an open access article distributed under the terms and conditions of the Creative Commons Attribution (CC BY) license (<http://creativecommons.org/licenses/by/4.0/>).